ACS APPLIED MATERIALS & INTERFACES

Research Article

www.acsami.org

Topography-driven bionano-interactions on colloidal silica nanoparticles

Amauri J. Paula,*[,†] Camila P. Silveira,[§] Diego Stéfani T. Martinez,[‡,∥] Antonio G. Souza Filho,[†] Fabian V. Romero,[¶] Leandro C. Fonseca,[‡] Ljubica Tasic,[¶] Oswaldo L. Alves,[‡] and Nelson Durán[§,#]

[†]Department of Physics, Universidade Federal do Ceará, P.O. Box 6030, 60455-900, Fortaleza, Ceará, Brazil

[§]Laboratory of Biological Chemistry, [¶]Department of Organic Chemistry, and [‡]Laboratory of Solid State Chemistry, Instituto de Química, Universidade Estadual de Campinas, P.O. Box 6154, 13083-970, Campinas, São Paulo, Brazil

[∥]Brazilian Nanotechnology National Laboratory, Centro Nacional de Pesquisa em Energia e Materiais, CNPEM, P.O. Box 6192, 13083-970, Campinas, São Paulo, Brazil

[#]Center of Natural and Human Sciences, Universidade Federal do ABC, 09210-580, Santo André, São Paulo, Brazil

Supporting Information

ABSTRACT: We report here that the surface topography of colloidal mesoporous silica nanoparticles (MSNs) plays a key role on their bionano-interactions by driving the adsorption of biomolecules on the nanoparticle through a matching mechanism between the surface cavities characteristics and the biomolecules stereochemistry. This conclusion was drawn by analyzing the biophysicochemical properties of colloidal MSNs in the presence of single biomolecules, such as alginate or bovine serum albumin (BSA), as well as dispersed in a complex biofluid, such as human blood plasma. When dispersed in phosphate buffered saline media containing alginate or BSA, monodisperse spherical MSNs interact with linear biopolymers such as alginate and with a globular protein such as bovine serum albumin (BSA) independently of the surface charge sign (i.e. positive or negative), thus leading to a decrease in the surface energy and to the colloidal stabilization of these nanoparticles. In contrast, silica nanoparticles with irregular surface topographies are not colloidally stabilized in the presence of alginate but they are electrosterically stabilized by BSA through a sorption mechanism that implies reversible conformation changes of the protein, as evidenced by circular dichroism (CD). The match between the biomolecule size and stereochemistry with the nanoparticle surface cavities characteristics reflects on the nanoparticle surface area that is accessible for each biomolecule to interact and stabilize any non-rigid nanoparticles. On the other hand, in contact with variety of biomolecules such as those present in blood plasma (55%), MSNs are colloidally stabilized regardless of the topography and surface charge, although the identity of the protein corona responsible for this stabilization is influenced by the surface topography and surface charge. Therefore, the biofluid in which nanoparticles are introduced plays an important role on their physicochemical behavior synergistically with their inherent characteristics (e.g., surface topography).

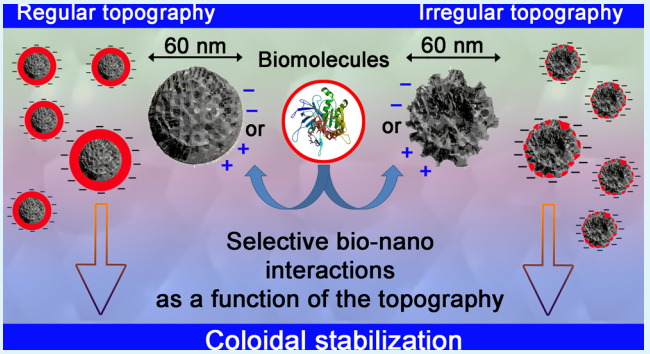

KEYWORDS: *mesoporous silica, colloidal nanoparticles, biomolecules interaction, bovine serum albumin, alginate, protein corona, human blood plasma*

1. INTRODUCTION

Silica nanostructures are very likely to be present in the next generation of nano-based products that will impact several technological areas, possibly benefiting from industrial processes to medical protocols. In particular, mesoporous silica nanoparticles (MSNs) operating under the host-guest approach can be used to improve the theranosis of several diseases, including cancer.[1−12] Consequently, there has been an increasing production of MSNs in combinations with other materials, with different morphologies and in different contexts of biomedical applications, result of a remarkable creativity of the scientific community. However, obtaining truly dispersible silica nanocarriers for specific nanobiotechnological applications (e.g., intravenous administration) is challenging mainly because of the composition and the ionic strength of physiological media.[13] In such cases, individualization of MSNs in the medium is necessary to provide homogeneity similar to a soluble molecular entity, an efficient circulation in the organism and also to prevent undesirable biological effects resulted from agglomeration.[14,15]

Received: December 5, 2013
Accepted: February 13, 2014
Published: February 13, 2014

Along with the stability issue, interactional phenomena manifested at the interface of the nanoparticle surface and the biological fluid is also a key point, since they will ultimately determine complex biological effects that will influence on both efficiency and toxicology of the silica nanocarriers. Both aspects are related to the interface phenomena, which emerge as a central issue to further advancing scientifically and technologically, not only for silica nanocarriers but also for nanoparticles (NPs) in general. Immediately after their introduction in the physiological environment (e.g. human blood plasma), proteins, such as albumin, fibrinogen, and vitronectin, adsorb on the nanoparticle surface (i.e. protein corona effect).[16−18] The formation of the biomolecular corona alters the size and interfacial composition of the nanoparticle, providing it a new biological identity which is then sensed by cells,[19−21] and finally influencing on cellular and physiological responses including signaling, membrane adhesion, uptake, translocation and toxicity.[22−25] For instance, by designing the biomolecular corona, it was recently showed that nanoparticles can acquire a selective targeting capacity for cancer cells, through a vitronectin-enriched protein corona adsorbed on the surface.[26]

Although there are studies in the literature associating the type of adsorbing biomolecules and protein corona formation as a function of the size, hydrophobicity, curvature, solubility, and aspect ratio of silica and other nanomaterials (mainly for human blood plasma biomolecules),[16,17,19,27−34] less attention has been given to the influence of the surface microchemical environment of the nanoparticle. In this context, a current and crucial open question on these bio-nano interactions raised in recent review articles is: what is the relationship between the structure of the biomolecule and the surface topography of the colloidal nanoparticle on which it is adsorbing?[19,32,35] Pioneer studies which dealt with this issue associated protein interaction and conformation changes with the topography difference resulted from rigid spherical-like colloidal nanoparticles with different sizes.[16,17,36,37] Hence they evaluated just curvature effects influencing on the biomolecule-nanoparticle interaction. To the best of our knowledge, there are no studies correlating bio-interactions to the colloidal nanoparticle topography tailored at a sub-ten-nanometer range and presenting sharp topographic contours. This lack of studies is possibly associated to synthetic issues that hamper the nanoparticle surface design within this size range.

Aiming to shed light on this complex issue, we studied the biophysicochemical interactions occurring at the interface of colloidal silica nanoparticles possessing very distinct surface topographies. The study of such fine interactions occurring at the bio-nano interface of porous silica nanoparticles can be currently benefited from the development of sol−gel methods achieved in the last years. These methods are capable of providing exclusive surface chemical modifications preserving the particle inner pores and their functionalities. Through a step addition of Si monomers (i.e. silicon alkoxides or organosilanes) that condense in different kinetic steps of the particle growth process in a sol−gel method, a hierarchical functionalization of colloidal MSNs can be achieved by co-condensing in the inner pores an organic group different from that co-condensed on the surface of the nanoparticle.[38,39] Furthermore, our group recently reported that the porous structure of MSNs can be modified through the addition of specific organosilanes, which lead to the increase in the pore size without impacting both size and colloidal stability of the silica nanoparticle,[40] thus allowing an accurate design of the surface microchemical environment, including the surface topography. Therefore, we were able to evaluate the influence of the nanoparticle surface charge and topography on the bionano-interactions manifesting in biofluids with different degrees of complexity: a solution of a single biomolecule (i.e. alginate or bovine serum albumin) and the blood plasma, which contains a myriad of biomolecules (>3700 proteins). From the experimental observations it was possible to evidence that the colloidal stability is strongly affected by short-range bionano-interactions that occur selectively from a matching mechanism between the surface cavities characteristics and the biomolecule size and stereochemistry.

2. MATERIALS AND METHODS

2.1. Synthesis of Porous Silica Nanoparticles with Spherical Morphology. The influence of the surface chemical groups and charge on the interaction with biomolecules was evaluated through the strict functionalization of the nanoparticle outer surface to generate antagonistic electrochemical environments (negatively and positively charged), as a function of the organosilanes used for the surface functionalization. These different microchemical environments would provide important insights regarding possible chemical interactions occurring between mesoporous silica nanoparticles (MSNs) and the analyzed biomolecules (i.e., alginate, BSA and human blood plasma). For the first case, the negatively charged surface, a hierarchical functionalization of the nanoparticle with propylmethylphosphonate (an ionizable group) was achieved by a sequential addition of the organosilane as a function of the reaction time. This co-condensation sol−gel method[40] was firstly conceived based on parameters used by Stöber et al.[41] and Bein et al.,[38,39] and it is suitable to produce monodisperse spherical porous silica nanoparticles with a size distribution of 40−80 nm and pore size around 2 nm. For this, 0.75 g of cetyltrimethylammonium bromide (CTAB) were dissolved in 20 mL of a NH_3 aqueous solution (0.05 mol L^{-1}) and the final solution was homogenized under magnetic stirring in a round-bottomed distillation flask attached to a reflux condenser at 5 °C (to avoid ethanol evaporation). To this solution, 3.2 mL of absolute ethanol were added as the cosolvent and the mixture was homogenized for 15 minutes at 60 °C. Subsequently, 2.5 mL of tetraethyl orthosilicate (TEOS, 11.2 mmol) were inserted and the flask was kept at the same temperature for 90 minutes under stirring. Then, 128 μL of 3-(trihydroxysilyl)-propylmethyl-phosphonate (THSPMP) were added to the mixture which was left under stirring at 60 °C for more 30 minutes, totalizing 2 h of synthesis. At this addition time used for THSPMP (t = 90 minutes) most of the silica monomers initially provided by TEOS were already condensed as nanoparticles, thus resulting just in an external functionalization of the nanoparticle during the last 30 minutes of reaction, while the internal porous structure was preserved. The quantity of THSPMP used is an excess of 2.5%-mol of Si based on the quantity of TEOS used (0.28 mmol). After the reaction is over, the product was isolated, resuspended in ethanol and washed to promote the CTAB extraction (see the Supporting Information for details). After the CTAB extraction procedure, the sample was washed twice with absolute ethanol, resuspended in absolute ethanol and stored in the refrigerator. This sample was named "spherical Si-$PMeO_3H$".

To obtain a positively charged surface on MSNs, a functionalization with 3-aminopropyl groups was carried out by a different process as the co-condensation of its respective organosilane (3-aminopropyl-triethoxysilane, APTES) induces a pH variation that leads to the production of elongated nanoparticles (aggregated). In this way, the surface modification was done by a post-grafting process of spherical silica nanoparticles containing silanol groups on the external surface (unfunctionalized), which were obtained through the method above-mentioned excluding the THSPMP addition step (at t=90 minutes). The grafting of APTES on these unfunctionalized nanoparticles was performed prior to the CTAB extraction. Residual CTAB present in the pores of the spherical MSNs before its extraction prevents the

attachment of APTES on the internal porous structure, thus restricting the functionalization on an external area of the nanoparticle. Therefore, 0.29 g of bare spherical silica nanoparticles containing CTAB were resuspended by sonication in 40 mL of absolute ethanol for 30 minutes and transferred to a round-bottomed distillation flask attached to a reflux condenser at 5°C. The suspension was homogenized under stirring for 15 minutes at 60°C and then 212 μL of APTES were added to the mixture (excess of 25%-mol of Si). The percentage of silicon (%-mol of Si) per gram of unfunctionalized spherical nanoparticles was estimated through thermogravimetric analyses by considering the residue above 850°C as being just silicon dioxide (see Figure S1 in the Supporting Information). The reaction was kept under stirring at 60°C for 2 h and at room temperature for 12 h. This sample was named "spherical Si−NH_2". After the reaction the product was isolated, resuspended in ethanol, washed (i.e., CTAB extraction) and finally resuspended in absolute ethanol following the same processes as already described for sample "spherical Si-$PMeO_3H$".

2.2. Synthesis of Porous Silica Nanoparticles with Irregular Morphology. To produce MSNs with irregular surface topography a process of co-condensation with phenyltriethoxysilane (PTES) was performed keeping constant other parameters used for the production of the unfunctionalized spherical silica nanoparticles. In the supramolecular arrangement formed in the reaction medium this organosilane leads to the increase in the size of the micelles, thus generating larger pores and preserving the monodisperse feature of nanoparticles. For this, 1.49 mL of TEOS was mixed with 816 μL of PTES and sonicated for 15 minutes (totalizing 11.2 mmol of Si). The mixture was then transferred to the distillation flask at the same conditions as previously described (i.e. quantities of the NH_3 solution, CTAB and ethanol, and temperature and reaction time). This first addition of Si precursors (at t = 0 min) promotes the particle nucleation and growth. After 60 minutes, time at which the majority of Si monomers had already been condensed another TEOS addition (124 μL) was performed to isolate the internal hydrophobic pores (functionalized with phenyl groups) from the external surface which is further functionalized with hydrophilic groups. Thus, an unfunctionalized silica shell was created from 60 to 90 minutes of reaction. The last TEOS addition (124 μL, at t = 90 min) was done to complete the formation of the outer surface of the nanoparticle. The negative surface functionalization with propylmethylphosphonate groups was done during the formation of this outer shell of silica, from 90 to 120 minutes of reaction. In this way, the organosilane (THSPMP, 128 μL, 0.28 mmol) was inserted immediately after the last TEOS addition (at t = 90 min). This product was named "irregular Si-$PMeO_3H$". After the end of the reaction the product was isolated, resuspended in ethanol, washed (i.e., CTAB extraction), and finally resuspended in absolute ethanol following the same processes as already described.

MSNs with irregular morphology were also functionalized with 3-aminopropyl groups through a post-grafting process on irregular silica nanoparticles possessing silanol groups on the external surface and containing CTAB. This nanoparticle was obtained similarly to sample "irregular Si-$PMeO_3H$" excluding the THSPMP addition step (at t=90 minutes) and preserving the CTAB in the pores. Therefore, approximately 0.20 g of these irregular nanoparticles with an unfunctionalized external surface were resuspended by sonication in 35 mL of absolute ethanol for 30 minutes and transferred to a round-bottomed distillation flask attached to a reflux condenser at 5°C. To the suspension, 95.7 μL of APTES were added (excess of 20%-mol of Si calculated through thermogravimetric analyses). Experimental procedures used here were the same as those used for obtaining sample "spherical Si-NH_2". After the synthesis the product ("irregular Si−NH_2") was isolated, resuspended in ethanol, washed (CTAB extraction) and finally resuspended in absolute ethanol following the same processes as already described. The reagent list and a summary of the parameters used for the syntheses and functionalizations of MSNs are presented in the Supporting Information. For all syntheses performed (MSNs with both spherical and irregular morphology) yields were superior to 70%.

2.3. Adsorption, Colloidal Stability, and Protein Corona Assays. To evaluate the zeta potential and colloidal stability of spherical and irregular monodisperse MSNs in the presence of alginate and bovine serum albumin (BSA), assays were performed using a MSNs suspension of 0.25 mg mL^{-1} for all samples. The stored alcoholic suspensions were centrifuged, washed twice with deionized water, and resuspended in deionized water (through sonication) for the physicochemical assays. In the 10×-diluted phosphate buffered saline (PBS) solution used for experiments (1.0 mmol L^{-1} of a phosphate buffer, 0.27 mmol L^{-1} of potassium chloride and 13.7 mmol L^{-1} of sodium chloride; pH 7.4), spherical and irregular nanoparticles with 3-aminopropyl (Si-NH_2) groups on the external surface were not stable, sedimenting minutes after their addition. In contrast, nanoparticles with propylmethylphosphonate groups (Si-$PMeO_3H$) on the surface were long-term stable in this medium. Biomolecules were dissolved in this PBS solution (10×-diluted) yielding concentrations of alginate and BSA that ranged from 0.1 μg mL^{-1} to 0.50 mg mL^{-1}. Interaction of alginate and BSA with MSNs (spherical and irregular) was evaluated through zeta potential (ζ) measurements in solutions containing this concentration range of biomolecules. The colloidal stability was evaluated through a centrifugation study carried out in a PBS solution containing 0.50 mg mL^{-1} of biomolecules at relative centrifugal forces (rcf) of 94, 2348, 9391, and 18 407 (for 5 minutes). Quantification of suspended MSNs was done by withdrawing a volume from the supernatant after the centrifugation and by measuring its light absorption at 263 nm (see Figure S2 in the Supporting Information). The measured absorbance was subtracted from the absorbance of the biomolecule solution in PBS without the nanoparticles, finally yielding the percentage result given in the graphics. Silica nanoparticles used in this study (spherical and irregular) at 0.25 mg mL^{-1} are barely stable in the presence of alginate at 0.50 mg mL^{-1} dissolved in 1x-diluted PBS. Under this circumstance, nanoparticles sediment at relatively low centrifugation velocities (up to 1000 rcf). In this way, only through the dilution (to 10×) it was possible to obtain clear evidences of the dependence of the surface topography on the colloidal stabilization.

Evolution of the BSA chemical structure as a function of the incubation time with porous silica nanoparticles was carried out through far-UV circular dichroism (CD) spectroscopic analysis. CD response for the protein arises from its α- and β-helix secondary structures. The loss of the α-helix structure (predominant over β) after interaction with silica nanoparticles as well as the amount of protein adsorbed were estimated by analyzing the degree of molar ellipticity $[\theta]$ at 208 nm. For these assays, spherical and irregular silica nanoparticles in a concentration of 0.25 mg mL^{-1} were incubated in a 0.50 mg mL^{-1} solution of BSA (dissolved in a 10×-diluted PBS solution, pH of 7.4) for 5, 30, 60, and 180 minutes. After the incubation suspensions were then centrifuged at 18 407 rfc (4°C) for 30 minutes to isolate nanoparticles. CD spectroscopy was performed with a volume of the supernatant withdrawn from the vials after centrifugation. A relative content of α-helix structure (%) was estimated by correlating the $[\theta]$ magnitude at 208 nm in BSA spectra, after the incubation with MSNs, to the $[\theta]$ value obtained for a pure 0.50 mg mL^{-1} BSA solution. An estimate of BSA adsorption on MSNs was also obtained through the same method, considering that the decrease in $[\theta]$ at 208 nm for MSNs incubated with BSA resulted from the BSA adsorption and not from the loss of the α-helix secondary structure, as it is further discussed. Another single CD reading was performed with the nanoparticles suspended in the presence of BSA. For this measure, spherical and irregular MSNs (0.25 mg mL^{-1}) were incubated with BSA (0.50 mg mL^{-1}) for 60 minutes before the analysis. More details regarding CD spectroscopy are given in the Supporting Information. ζ-potential and colloidal stability results, as well as CD spectra presented here are the average of at least three independent measurements.

Proteins from hard corona that strongly interacted with colloidal MSNs were extracted from the nanoparticles surface after their incubation in human blood plasma. Briefly, stock colloidal suspensions were prepared by sonicating MSNs (5.0 mg mL^{-1} in deionized water) for 30 minutes in an ultrasound bath (Cole-Parmer 8891). After that,

nanoparticles (500 μg mL^{-1}) were incubated in human blood plasma (55%) for 1 h at 37°C by using Protein LoBind Eppendorf tubes (1.5 mL). Nanoparticles were then isolated by centrifugation (at 20,817 rcf for 1 h at 4°C), and resuspended in a 1x-diluted PBS solution (10.0 mmol L^{-1} of a phosphate buffer, 2.7 mmol L^{-1} of potassium chloride and 137 mmol L^{-1} of sodium chloride; pH 7.4). Three washing processes with the PBS solution were performed in order to remove weakly-bond biomolecules (centrifugation in this step was performed at 20 817 rcf for 30 min at 4°C). Finally, the pellets (MSNs containing hard corona proteins adsorbed) were resuspended in a protein loading buffer (150 μL, containing 62.5 mM of Tris-HCL, 2% (w/v) of SDS, 10% of glycerol, and 0.01% (w/v) of bromophenol blue; pH 6.8) and boiled for 3 minutes at 100°C. From this resulting suspension, 15 μL was loaded in a 15% SDS-polyacrylamide gel (1D SDS-PAGE). Experiments were also performed standardizing the MSNs BET surface area (at 800 m^2 g^{-1}). After running the electrophoresis, the gel was stained with the coomassie blue staining.

3. RESULTS

By using the synthetic platform above-mentioned,[38−41] we were able to produce functionalized colloidal MSNs with the same size (40−80 nm as determined by transmission electron microscopy [TEM], see Figures S3a and S3b in the Supporting Information) but very distinct surface topographies: a spherical silica nanoparticle with small pores (~2 nm) and an irregular nanoparticle with wide-open pores on the surface (>5 nm), thus resulting in larger pore volumes (see Figure S4 in the Supporting Information). The increase in the pore size was achieved by replacing up to 30%-mol of Si from tetraethyl orthosilicate (TEOS), the main source of Si, by phenyl-triethoxysilane (PTES) in the first addition of silicon monomers. Substitution of 40%-mol of Si by this organosilane induces the loss of the nanoparticle monodispersity characteristic. Furthermore, the surface of both MSNs was exclusively modified by using 3-aminopropyl-triethoxysilane and 3-(trihydroxysilyl)-propylmethylphosphonate, which ionize at physiological pH (7.4) generating positive and negative surface charges, respectively. The outer surface functionalization of the colloidal MSNs with aminopropyl and propylmethylphosphonate groups was confirmed through ^{13}C nuclear magnetic resonance (NMR) in the cross-polarization and magic angle spinning mode (CPMAS, see Figures S5 and S6 in the Supporting Information), and ζ potential measurements in a 1.0 mmol L^{-1} KCl solution (see Table 1). The external functionalization was confirmed through the identification of carbon atoms for each chemical group in ^{13}C NMR spectra. The presence of these groups reflected in a variation of the surface charge for each sample: samples Si-NH$_2$ (with spherical or irregular morphology) have positive ζ-potential values whereas samples Si-PMeO$_3$H present negative ζ-potential.

The porous structure of the colloidal MSNs was revealed by scanning transmission electron microscopy (STEM) in the high-angle annular dark-field mode (HAADF), as shown in Figure 1. The very distinct surface topography as a result of different pore structures between the two samples was observed in the micrographs: apparent radial pores around 2 nm for MSNs with spherical morphology (see Figure 1a) and pores larger than 5 nm for MSNs with irregular morphology (see Figure 1b). As can be observed, these nanoparticles are not rigid spherical-like nanoparticles. Instead, they are irregular nanoparticles with complex porous structures. In particular, pores in the irregular silica nanoparticles are distributed in an apparent fractal arrangement, with the pore sizes varying along the NPs radius, from the center to the outer surface (see Figure 1b). In this way, besides both nanoparticles (i.e. regular and irregular) have similar sizes, they will interact differently with a molecule (or biomolecule) once the accessible surface area for this specific molecule may be quite different depending on its size and stereochemistry. For instance, a small polypeptide interacting with the irregular silica nanoparticles used here will have a larger accessible surface area (ASA) for chemical

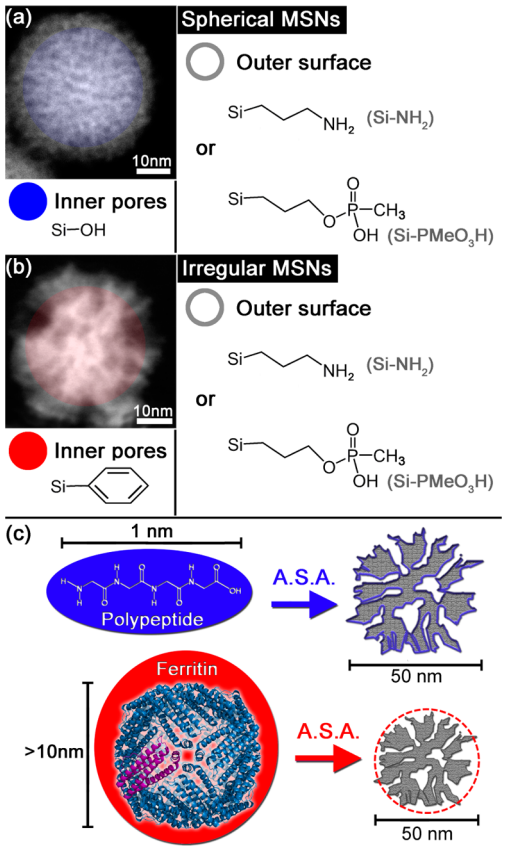

Figure 1. Scanning transmission electron microscopy images in the high-angle annular dark-field mode (HAADF-STEM) of the hierarchically functionalized MSNs with (a) spherical and (b) irregular morphology. Diagrams illustrating the hierarchical organic functionalizations present in MSNs are also represented. Samples were named according to the outer surface functionalization as given in parentheses. (c) Diagram illustrating the accessible surface area (A.S.A.) of an irregular nanoparticle for a small polypeptide and a large protein such as ferritin (represented in blue and red, respectively).

Table 1. Physicochemical Characteristics of Colloidal MSNs

sample	surface area[a] (m^2 g^{-1})	pore volume[b] (cm^3 g^{-1})	zeta potential (ζ)[c] value (mV)	zeta potential (ζ)[c] STD (mV)[d]
		spherical MSNs		
Si-NH$_2$	624	0.9	+14.1	4.6
Si-PMeO$_3$H	773	1.1	−30.3	7.6
		irregular MSNs		
Si-NH$_2$	923	1.8	+17.7	4.9
Si-PMeO$_3$H	950	2.1	−30.5	6.8

[a]Results from the N$_2$ adsorption branch using the BET method. [b]Evaluated through the single-point value adsorbed at P/P_0 = ~0.94. [c]Measured with a nanoparticle suspension in a 1 mmol L^{-1} KCl solution. [d]STD = standard deviation.

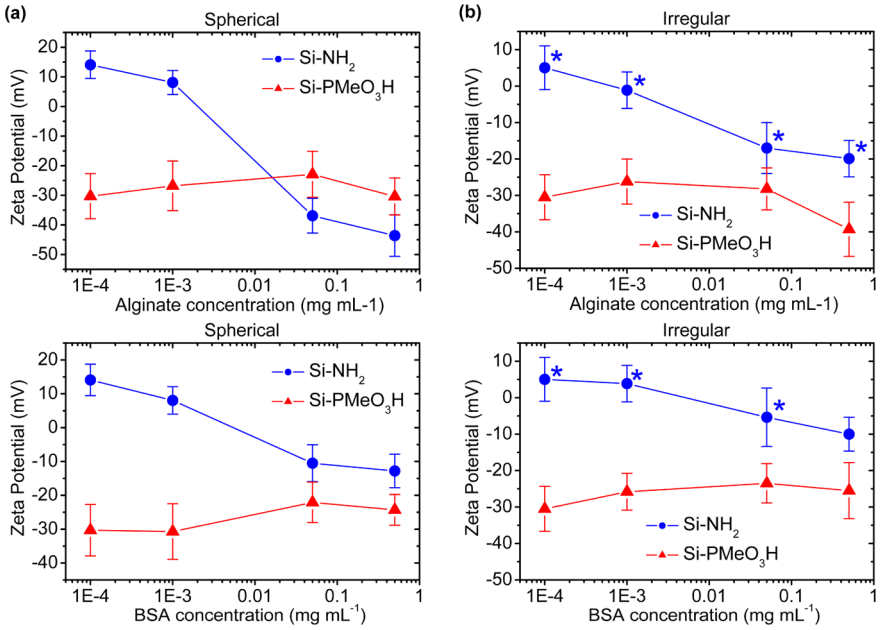

Figure 2. ζ potentials of hierarchically functionalized MSNs with (a) spherical and (b) irregular morphologies in a 10×-diluted PBS solution measured as a function of the concentration of alginate and BSA and as a function of the functionalizing groups on the external surface. The MSNs concentration in all studies was of 0.25 mg mL^{-1}. Asterisks stand for unstable suspensions of MSNs.

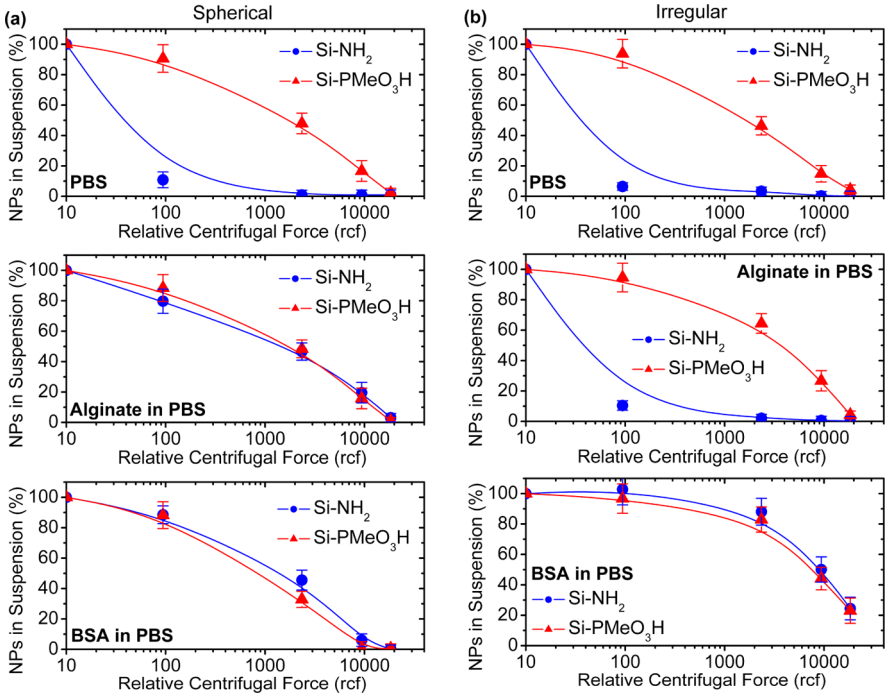

Figure 3. Colloidal stability assays for (a) spherical and (b) irregular silica nanoparticles in a 10×-diluted PBS solution (PBS), in a 0.50 mg mL^{-1} alginate solution in PBS (alginate in PBS), and in a 0.50 mg mL^{-1} BSA solution in PBS (BSA in PBS). The MSNs concentration in all studies was of 0.25 mg mL^{-1}.

interaction compared to a protein such as ferritin (see Figure 1c). For both biomolecules mentioned, the accessible surface area is different from the BET surface area which has been commonly used as the normalization parameter for interaction studies that uses rigid nanostructures with different morphologies. Therefore, for non-rigid spherical-like nanoparticles in the presence of a mixture of molecules (or biomolecules), the accessible surface area will vary for each molecule. In this specific study, as regular and irregular silica nanoparticles have approximately the same diameter (see Figure 1), we have performed all interaction experiments using the nanoparticle concentration in mg mL^{-1} instead of BET surface area per mL.

Diagrams represented in Figure 1 also show the surface and pore functionalizations. Deprotonation of propylmethylphosphonate groups (Si-$PMeO_3H$) leads the nanoparticle surface charge to become negative at pH 7.4, provided by a PBS solution. In contrast, protonation of the propylamine groups (Si-NH_2) leads to a positively charged surface. Regardless of the

dx.doi.org/10.1021/am405594q | ACS Appl. Mater. Interfaces 2014, 6, 3437−3447

Table 2. DLS Measurements of Colloidal MSNs

	Bare MSNs[a]		MSNs in alginate[c]		MSNs in BSA[c]	
sample	average size (nm)	PDI	average size (nm)	PDI	average size (nm)	PDI
			spherical			
Si-NH_2	121 ± 9	0.09	311 ± 20	0.18	214 ± 19	0.21
Si-$PMeO_3H$	135 ± 11	0.11	194 ± 21	0.19	255 ± 20	0.22
			irregular			
Si-NH_2	117 ± 9	0.08	[d]	[d]	233 ± 21	0.20
Si-$PMeO_3H$	120 ± 13	0.11	[e]	[e]	224 ± 19	0.19

[a]Analyses carried out in deionized water since most of the suspensions of bare silica nanoparticles were unstable in PBS. [c]Measurements carried out in a 10×-diluted PBS solution containing 0.25 mg mL^{-1} of MSNs and 0.50 mg mL^{-1} of the biomolecule. [d]Unstable colloidal suspension; unable to measure. [e]High polydispersity index (>0.40). The results presented are the average of at least four independent measurements.

morphology (spherical or irregular) nanoparticles with Si-NH_2 surface groups were not long-term stable in the 10×-diluted PBS solution used for all physico-chemical studies, in which MSNs sediment minutes after their dispersion. Surface functionalization with propylmethylphosphonate groups provides a substantial increase in the colloidal stability of MSNs, as already reported,[40] for both surface topographies used in this study.

Alginate and BSA are both negatively charged biomolecules at pH 7.4; with a pKa and an isoelectric point around 3.5 and 4.6 (at 25°C), respectively.[42,43] Their adsorption on colloidal MSNs in PBS medium (10x-diluted) was evaluated by measuring the zeta potential (ζ) of MSNs as a function of the biomolecule concentration (see Figure 2). For amine-grafted spherical silica nanoparticles (spherical Si-NH_2, see Figure 2a), ζ-potential values changed the sign from positive to negative at a weight-ratio of 1:5 for both alginate:MSNs and BSA:MSNs dispersions (0.05 mg mL^{-1} of biomolecule:0.25 mg mL^{-1} of MSNs), thus indicating the adsorption of the biomolecules at these conditions. Negatively charged spherical MSNs (spherical Si-$PMeO_3H$) did not present a linear variation of ζ-potential values as a function of the increasing amount of biomolecules (alginate or BSA, see Figure 2a). As for MSNs with an irregular morphology, the alginate presence in a weight-ratio of up to 2:1 (alginate/MSNs) did not lead to the stabilization of the nanoparticles with amines on the surface (Si-NH_2), which sediment minutes after their dispersion in the PBS solution (see Figure 2b). In addition, BSA did lead to the stabilization of these irregular MSNs (Si-NH_2) at a biomolecule:MSNs weight-ratio of 2:1 for sample Si-NH_2, resulting in negatively charged nanoparticles. By measuring the zeta potential of these colloidally unstable irregular MSNs it was also possible to identify the surface charge inversion for the positively charged Si-NH_2 MSNs as a function of the concentration of biomolecules (alginate and BSA), even though the measured value is not a result of the electrophoretic mobility of individualized nanoparticles, but of aggregates (see Figure 2b). Phosphonate-functionalized irregular MSNs (irregular Si-$PMeO_3H$) were colloidally stable in PBS medium regardless the alginate and BSA concentration, thus possessing negative ζ values (around −30 mV) for all concentrations used.

To assess the effects of the alginate and BSA interactions on the MSNs surface the colloidal stability of the nanoparticles was evaluated through a centrifugation study. The percentage of suspended nanoparticles was quantified by measuring their UV-visible light absorption at 263 nm, which is related strictly to the suspended silica. The colloidal instability of both spherical and irregular Si-NH_2 was observed at a relative centrifugal force (rfc) of 94 (see Figure 3). At this same rcf value phosphonate-functionalized colloidal MSNs with spherical and irregular morphologies were very stable, although they do sediment at 18 407 rcf. Interactions with both alginate and BSA lead to an increase in the colloidal stability of spherical Si-NH_2, becoming similar to the stability of spherical Si-$PMeO_3H$ (see Figure 3a). In addition, MSNs with irregular morphology were not stabilized in the presence of alginate in the PBS medium (10×-diluted), in which they sediment at low rcf values even at an alginate:MSNs weight-ratio of 2:1 (see Figure 3b). However, BSA interacting with irregular Si-NH_2 nanoparticles at a BSA:MSNs weight-ratio of 2:1 led to a surprising increase in their colloidal stability (see the bottom panel of Figure 3b). In fact, phosphonate-modified nanoparticles (irregular Si-$PMeO_3H$) were also more stable in the presence of BSA, not sedimenting completely even at 18 407 rcf (for 5 minutes). This colloidal stabilization is a result of an electrosteric stabilization related to a short-range interaction between the biomolecule (alginate or BSA) and the nanoparticle. If they were stabilized exclusively by depletion mechanisms, which do not involve this short-range interaction but instead a long-range interaction with high molecular-weight polymers possessing determined chain lengths,[44] the stability behavior for irregular silica nanoparticles interacting with alginate (see Figure 3b, middle panel) should be the same as that of spherical nanoparticles interacting with this same biomolecule (see Figure 3a, middle panel). The same observation applies for spherical and irregular nanoparticles interacting with BSA (see Figure 3a and 3b, bottom panels). This topography effect has not been described so far because the majority of studies presented in the literature focused on the interaction of biomolecules with nanomaterials possessing rather smooth and regular surfaces (i.e. rigid spherical nanoparticles).[16,17,19,28−31]

The uniformity of silica nanoparticle dispersions as a function of the surface functionalization was confirmed through the average size and polydispersity index (PDI) values, which were obtained through dynamic light scattering (DLS) measurements for nanoparticles with both spherical and irregular morphologies (Table 2). Since most of the samples produced were colloidally unstable in the PBS solution, except those functionalized with propylmethylphosphonate groups, DLS analyses of bare nanoparticles were performed in deionized water. When dispersed in the 10×-diluted PBS solution containing alginate or BSA in a 2:1 weight-ratio (0.50 mg mL^{-1} of biomolecule:0.25 mg mL^{-1} of MSNs) the average size for nanoparticles with spherical morphology was increased in the presence of both alginate and BSA, along with an increase in the PDI value. As irregular Si-NH_2 MSNs were not stabilized by alginate, a proper evaluation of average size could not be done through DLS. Interaction between irregular Si-$PMeO_3H$

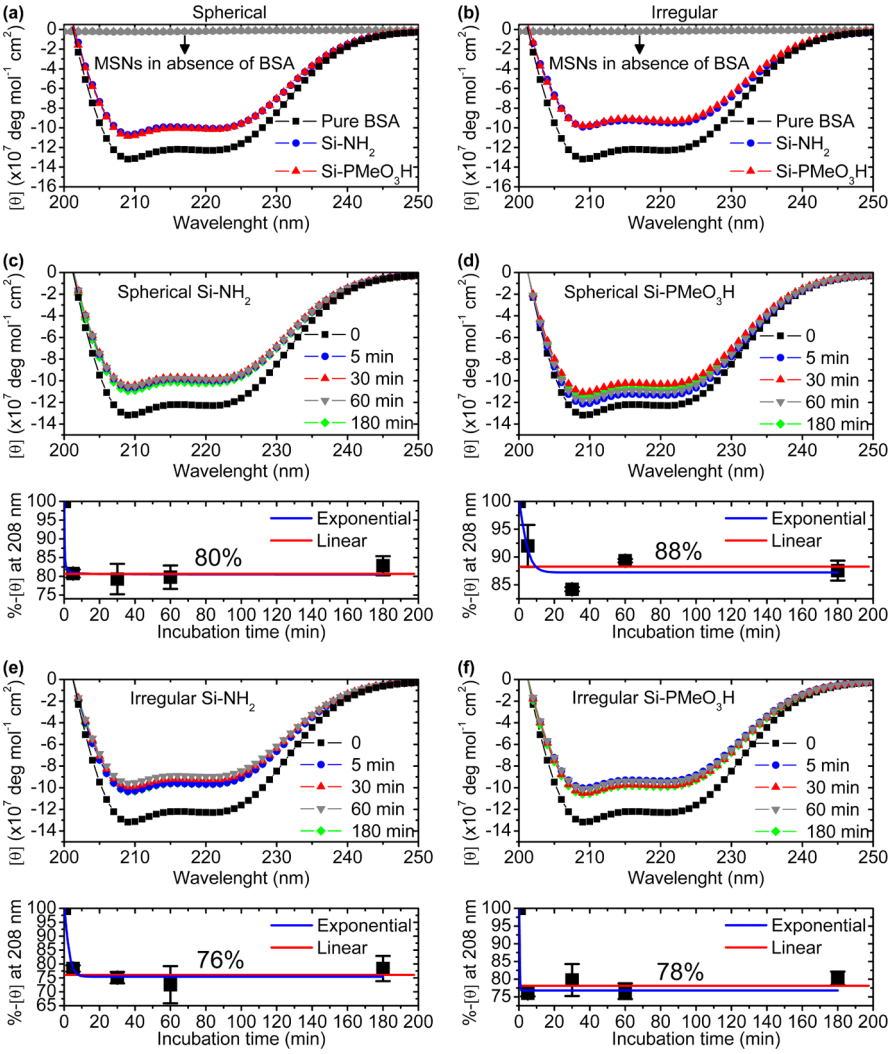

Figure 4. Circular dichroism (CD) spectra of MSNs suspensions with (a) spherical and (b) irregular morphologies in the presence and absence of BSA. CD spectra measured at the supernatant of centrifuged suspensions of (c and d) spherical and (e and f) irregular MSNs after their incubation with BSA for 5, 30, 60, and 180 minutes. The variation of the $[\theta]$ magnitude at 208 nm (given in %) is given at the bottom for each MSNs (spherical [c and d] and irregular [e and f]). Fits (linear and exponential decay) performed in these graphs provide an estimate of BSA adsorbed on MSNs. Spectra represented by 0 in c–f are the same as those represented by "Pure BSA" in a and b.

and alginate leads to the formation of non-uniform dispersions (i.e. polydispersions). As for irregular MSNs interacting with BSA (2:1 BSA:MSNs weight-ratio), their average size and polydispersity index did increase for both samples (Si-NH_2 and Si-$PMeO_3H$).

Insights regarding the MSNs interaction with BSA can be obtained through the analysis of the protein chemical structure through circular dichroism (CD) spectroscopy. As bare MSNs did not polarize far-UV radiation (see grey symbols in Figures 4a and 4b), it was possible to determine if the BSA adsorption on MSNs induces conformation changes in the protein. The spectrum of pure BSA was obtained after the centrifugation of the BSA solution (0.50 mg mL^{-1}) at 18 407 rcf for 30 minutes, and it is in accordance with previous results reported in the literature.[45] Decrease in $[\theta]$ intensities for both spherical and irregular MSNs with positively and negatively charged surfaces indicates that their interaction with BSA leads to a modification of the protein conformation, resulting mainly in the loss of α-helix structure (see Figures 4a and 4b). Instead of an adsorption process, if BSA is forming a complex with silica nanoparticles and thus if it is being irreversibly denatured by this interaction, a time-resolved CD spectrum of BSA would reveal the phenomenon by changing its features or decreasing its intensity as a function of the interaction (i.e., incubation) time, considering the dynamic nature of the interaction kinect process.[36,45−47] However, as observed in CD spectra measured at the supernatant of the centrifuged MSNs suspensions (see Figure 4–f), the spectrum shape after incubation with MSNs for 5, 30, 60, and 180 minutes did not change and the ratio between $[\theta]$ values at 208 and 220 nm was preserved as a function of the time. Spectra represented by 0 in Figure 4–f are the same as those represented by "Pure BSA" in Figure 4a and b. Thus, results indicate that the BSA structural modification is reversible to the sorption process in which the proteins continuously adsorb and desorb on the nanoparticle surface. This conclusion drawn for porous silica nanoparticles is aligned with other studies showing that smaller (<60 nm) rigid spherical-like silica nanoparticles induce less or no permanent conformation changes in proteins compared to larger ones.[36,37] In this context, the decrease in the $[\theta]$ magnitudes for incubated BSA solutions compared to pure BSA is related to the amount of protein adsorbed on the nanoparticle surface

dx.doi.org/10.1021/am405594q | ACS Appl. Mater. Interfaces 2014, 6, 3437−3447

that was removed through the centrifugation. These $[\theta]$ values for incubated BSA are similar to those obtained in CD spectra acquired with MSNs suspended in the BSA solution (see Figure 4a and b).

As the BSA concentration is different for each CD measurement once a partial amount of the protein was adsorbed on the centrifuged nanoparticles, it was not possible to estimate the relative α-helix content following Lús method.[45,48] However, by comparing the spectrum of pure BSA (0.50 mg mL^{-1}) with those obtained for BSA solutions after the incubation one can estimate the amount of BSA adsorbed on silica nanoparticles as a function of the surface charge sign and topography. This value was obtained through the linear fitting (with zero slope) of the degree of molar ellipticity $[\theta]$ at 208 nm for all incubation times (from 5 to 180 minutes), which is equivalent to the $[\theta]_{208\ nm}$ average value for each set of $[\theta]_{208\ nm}$ values. As observed in the lower traces of Figure 4, exponential decay functions (i.e. a typical saturation curve for BSA adsorption[49]) fitted for incubation times from t = 0 (100% − θ_{208nm}) to 180 minutes tend to the lines fitted from 5 to 180 minutes with a maximum deviation of 1% between the two fittings.

As the BSA adsorption estimates in Figure 4−f (lower traces) are provided for nanoparticles with different accessible surface areas, it was not possible to perform an accurate comparison among them in the sense of on which sample there is a larger adsorption. Roughly, by considering that the $[\theta]_{208nm}$ intensity loss in CD spectra (see Figure 4c−f) was constant as a function of the incubation time, and that this loss was approximately the same for all MSNs (spherical and irregular), it was possible to calculate an adsorption ratio of 0.40 mg of BSA per mg of MSNs (40% w/w), which would correspond to a multilayer adsorption all over the nanoparticle surface, considering that all surface area is accessible for adsorption. However, by knowing that the accessible surface area is unknown for both spherical and irregular nanoparticles, a precise evaluation of the protein insertion into the surface cavities cannot be accurate calculated once the coverage ratio of BSA on MSNs is unknown. Regardless of this point, it is important to mention that the %-weight ratio estimated here is a much higher value compared to the BSA adsorption on rigid-like spherical silica nanoparticles with sizes around 35 nm (10%-weight).[50]

In a medium with a higher degree of complexity such as the blood plasma (55%), which contains a myriad of biomolecules, MSNs were colloidally stabilized regardless of their surface topography and charge. Although this stabilization is visually observed with the suspensions at rest, quantifying this colloidal stabilization is not feasible once it is difficult to obtain an individual and clear signal (e.g. through spectroscopic techniques) of the nanoparticle suspended in a complex medium such as the human blood plasma. In this medium, colloidal stabilization by depletion forces must also be considered along with steric and electrosteric stabilizations, once there are macromolecules with high molecular weights (>100 kDa) and in high concentration compared to MSNs. ζ potentials of the protein-coated nanoparticles were measured after centrifugation (20,817 rcf for 1 h at 4°C) and redispersion of nanoparticles in 10×-diluted PBS. All samples (spherical and irregular silica nanoparticles) were found to be negatively charged with potentials below −20 mV, with no significant differences among samples. Insights regarding the biomolecules involved in steric and electrosteric stabilization could be obtained by extracting the proteins which have strongly adsorbed on MSNs after 1 h of incubation with blood plasma (55%). Therefore, it was possible to reveal the identity of proteins present in the hard corona as a function of the surface topography and surface charge. The identification of these proteins was performed through sodium dodecyl sulfate polyacrylamide gel electrophoresis (SDS-PAGE), which indicated the existence of selective interactions in blood plasma (see Figure 5). Proteins with a molecular weight (MW) from

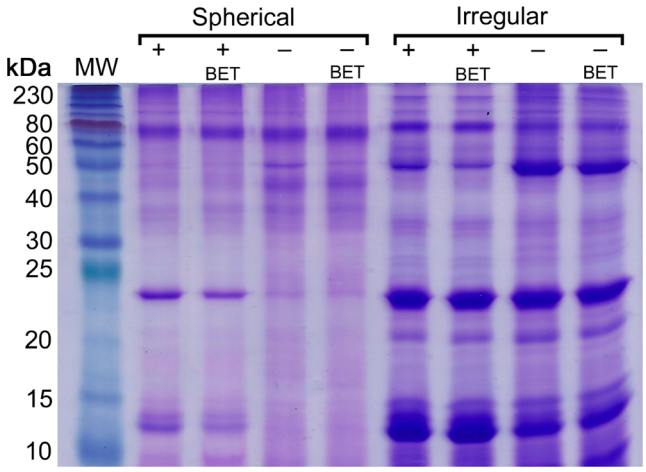

Figure 5. SDS-PAGE of the hard corona proteins extracted from spherical and irregular MSNs functionalized with amine and propylmethylphosphonate groups after their incubation with blood plasma. "+" stands for Si-NH_2 samples and "−"stands for Si-$PMeO_3H$ samples. Experiments were also performed standardizing the MSNs BET surface area (this result is shown in "BET" columns for each sample).

30 to 230 kDa interacted with both spherical and irregular silica nanoparticles. However, it was observed a selective adsorption of proteins with lower molecular weights (below 30 kDa), which largely interacted with irregular silica nanoparticles compared to spherical ones. Furthermore, between spherical silica nanoparticles with opposite surface charges, it was also observed a larger adsorption of these proteins (below 30 kDa) on Si-NH_2 MSNs. The presence of major bands between 50−230 and 20−25 kDa observed here mainly for irregular MSNs was previously observed for rigid-spherical-like silica nanoparticles.[31] For this experiment in particular, standardization in respect to the BET surface area was performed and results (see BET columns in Figure 5) indicated no substantial difference in the protein corona extracted after the incubation with blood plasma (55%).

4. DISCUSSION

Alginate, with a molecular weight ranging from 75 to 100 kDa can be kept at the nanoparticle−fluid interface mainly through electrostatic interactions manifested on positively charged MSNs (Si-NH_2). Similarly, BSA (M.W. of approximately 66 KDa) can interact with samples Si-NH_2 (spherical and irregular) through this same mechanism. Therefore, to the electrostatic interactions occurring in pH 7.4 between the oppositely-charged entities, the colloidal stability for spherical Si-NH_2 was increased with the presence of both alginate and BSA (see Figure 3a), which stabilize the nanoparticles through an electrosteric effect in the extent of that promoted by propylmethylphosphonate groups (spherical Si-$PMeO_3H$). Although the colloidal stability of sample spherical Si-

$PMeO_3H$ did not vary in the presence of alginate and BSA, the biomolecules can interact with the nanoparticles even when both entities present similar charges, because of the manifestation of hydrogen bonds and van der Waals forces. This effect was recently presented in a study that evaluated the adsorption of polypeptides on rigid-like silica nanoparticles as a function of their electrochemical features (i.e. cationic or anionic).[51] This study indicated that although there is a large adsorption of cationic polypeptides on negatively charged silica nanoparticles at pH 7 when the biomolecules are present in low concentrations, above a concentration threshold it was observed that anionic polypeptides also adsorb on the negatively-charged nanoparticle, thus confirming the role of hydrogen bonds and van der Waals forces on the interaction phenomenon (i.e. adsorption).

MSNs with irregular topographies did not have their colloidal stability altered in the presence of alginate even when there are electrostatic interactions occurring between sample irregular Si-NH_2 and this biomolecule, confirmed through the surface charge inversion (positive to negative) as the alginate concentration is increased (see Figure 2b). In contrast, BSA surprisingly stabilizes irregular MSNs which were unstable in the PBS medium used in this study (see Figure 3b, bottom panel). With dimensions of approximately 7.5 × 6.5 × 4.0 nm, interaction of this biomolecule on irregular MSNs could occur through the protein insertion in the surface cavities with a proper size matching, since the pores on the surface of these MSNs range from approximately 5 to 10 nm. Compared to rigid spherical-like silica nanoparticles, colloidal stabilization through the adsorption of calf serum proteins (in which BSA is the major component) on nonfunctionalized nanoparticles (~55 nm) was also reported,[52] and this stabilization appears to be directly related to the protein/NPs ratio: the larger is the ratio, the more nanoparticles are stable.[31,53] On the other hand, colloidal destabilization of smaller (~30 nm) rigid spherical-like silica nanoparticles in contact with BSA and fetal calf serum was also observed, thus indicating that the colloidal stabilization in the presence of biomolecules is also dependent on the nanoparticle size and curvature.[54]

By considering these results, it becomes evident that entropic aspects must be considered to explain this selective interaction of biomolecules as a function of the MSNs surface topography. Energetically unfavorable stereochemical changes of alginate can prevent the existence of an interaction such as observed for BSA on MSNs with an irregular topography, even when there could be enthalpic gains. This phenomenon was not observed when the same biomolecule interacts with more homogeneous surfaces (i.e. spherical MSNs), where it contributes for the decrease of the surface energy and leads to an electrosteric stabilization of the nanoparticle. In addition, interactional phenomena on surfaces with irregular topography can be energetically favored when there is a proper matching between the biomolecule size and stereochemistry (i.e. conformation), and the nanostructure surface force fields distribution.

An effect similar to that observed for the BSA:irregular MSN interaction was previously mentioned in simulations on particle-substrate interfacial interactions.[55] This study indicated that rough surfaces can present favorable sites for interaction with spherical nanometric entities as a result of the long range attractive van der Waals forces, which can be stronger than repulsive electrostatic forces in these sites. Because of the small number of atoms in a nanoparticle van der Waals forces are highly dependent on the surface distribution of these atoms, which strongly affects the interface interactions. Further computational analyses could be used to unveil the nature of this specific topography-driven interaction. However, some approaches that have been recently used for studying the interaction between peptides and silica nanoparticles with flat surfaces must be first modified to fit non-flat surfaces.[56]

Apart from this fundamental discussion regarding the nature of the topography-induced interaction occurring on MSNs, it is also important to consider the bio-effects that might manifest from this phenomenon. In a realistic context of application of MSNs, nanoparticles will interact with a huge variety of biomolecules such as those present in the blood plasma, and thus surface topography will influence on complex interactions based on size and stereochemistry matching mechanisms. These mechanisms result in the selectivity observed here in SDS-PAGE experiments for the hard corona extracted from MSNs after their incubation with blood plasma (see Figure 5). In this way, it is evident that the context in which nanoparticles are inserted exert a crucial role over their physicochemical properties. Furthermore, the biofluid which nanoparticles interact can completely modify the nanoparticle bio-effects through the formation of the biomolecular corona, which has important consequences for biomedical commercialization and regulation of nanomaterials. Examples of this situation have been reported recently by our group and others: the hemolytic effect induced by spherical MSNs with positively and negatively charged surfaces can be suppressed after their interaction with blood plasma proteins;[57] protein corona formed in cell culture media can alter the molecular diffusion process occurring in the pores of MSNs loaded with anticancer drugs, influencing on the delivery of drugs into cells;[58] and proteins from blood plasma can inhibit the targeting of functionalized nanoparticles.[59]

5. CONCLUSIONS

In summary, we report here a surface topography-stereochemical-selective interaction with colloidal silica nanoparticles containing different topographies. Firstly it was observed that the nanoparticle colloidal stability in the presence of alginate or BSA is more strongly related with the surface topography than the surface charge sign (i.e. positive or negative). While spherical-like porous silica nanoparticles with positively and negatively charged surfaces can be stabilized by alginate and BSA through an electrosteric mechanism, positively charged nanoparticles with irregular topography are stabilized through the interaction with BSA but not with alginate. Furthermore, it was evidenced that BSA has the ability to colloidally stabilize both nanoparticles (i.e. spherical and irregular) through short-range interactions that lead to a conformation change of the protein that is reversible as they desorb from nanoparticles. Further studies will definitely help to clarify the very peculiar characteristics of this type of interaction. Evaluation through fluorescent correlation spectroscopy, isothermal tritation calorimetry, differential centrifugal sedimentation and computational methods could be used for reaching this goal.

When dispersed in a more complex biofluid such as blood plasma, which contains a myriad of biomolecules (e.g. proteins) with different sizes and conformations, this influence of surface topography on the colloidal stabilization is suppressed, and both spherical and irregular silica nanoparticles are stabilized regardless of the surface charge sign (i.e. positive or negative). In this way, one becomes evident that the role of topography on the colloidal stabilization will be related with the very context in which nanoparticles are applied. It was also observed

that the group of proteins involved in this short-range interaction that influences on colloidal stabilization is different depending on the nanoparticle surface topography and the surface charge. This means that the protein corona identity for colloidal silica nanoparticles will vary according to these parameters. However, for nanoparticles with irregular surface topography, compared to spherical ones, it was evidenced a smaller variation of the hard corona proteins as a function of the surface charge (i.e. positive or negative).

■ ASSOCIATED CONTENT

Supporting Information

More details regarding the synthesis and characterization protocols, NMR spectra, thermogravimetric analyses, N_2 adsorption-desorption isotherms, and TEM micrographs. This information is available free of charge via the Internet at http://pubs.acs.org/.

■ AUTHOR INFORMATION

Corresponding Author

*Tel.: +55 85 3366 9008. E-mail: amaurijp@gmail.com; amaurijp@fisica.ufc.br.

Notes

The authors declare no competing financial interest.

■ ACKNOWLEDGMENTS

The authors thank the financial support from FAPESP, CNPq, INCT-Inomat, INCT-NanoBioSimes, and the Brazilian Nanotoxicology (CIGeNanotox-CNPq), Procad-CAPES, and Nanobiotec-CAPES Network Programs.

■ REFERENCES

(1) Vallet-Regi, M.; Ramila, A.; del Real, R. P.; Perez-Pariente, J. A New Property of MCM-41: Drug Delivery System. *Chem. Mater.* **2001**, *13*, 308−311.

(2) Lu, J.; Liong, M.; Zink, J. I.; Tamanoi, F. Mesoporous Silica Nanoparticles as a Delivery System for Hydrophobic Anticancer Drugs. *Small* **2007**, *3*, 1341−1346.

(3) Ashley, C. E.; Carnes, E. C.; Phillips, G. K.; Padilla, D.; Durfee, P. N.; Brown, P. A.; Hanna, T. N.; Liu, J. W.; Phillips, B.; Carter, M. B.; Carroll, N. J.; Jiang, X. M.; Dunphy, D. R.; Willman, C. L.; Petsev, D. N.; Evans, D. G.; Parikh, A. N.; Chackerian, B.; Wharton, W.; Peabody, D. S.; Brinker, C. J. The Targeted Delivery of Multicomponent Cargos To Cancer Cells by Nanoporous Particle-Supported Lipid Bilayers. *Nat. Mater.* **2011**, *10*, 389−397.

(4) Lee, J. E.; Lee, N.; Kim, T.; Kim, J.; Hyeon, T. Multifunctional Mesoporous Silica Nanocomposite Nanoparticles for Theranostic Applications. *Acc. Chem. Res.* **2011**, *44*, 893−902.

(5) Veeranarayanan, S.; Poulose, A. C.; Mohamed, M. S.; Varghese, S. H.; Nagaoka, Y.; Yoshida, Y.; Maekawa, T.; Kumar, D. S. Synergistic Targeting of Cancer and Associated Angiogenesis Using Triple-Targeted Dual-Drug Silica Nanoformulations for Theragnostics. *Small* **2012**, *8*, 3476−3489.

(6) Ashley, C. E.; Carnes, E. C.; Epler, K. E.; Padilla, D. P.; Phillips, G. K.; Castillo, R. E.; Wilkinson, D. C.; Wilkinson, B. S.; Burgard, C. A.; Kalinich, R. M.; Townson, J. L.; Chackerian, B.; Willman, C. L.; Peabody, D. S.; Wharton, W.; Brinker, C. J. Delivery of Small Interfering RNA by Peptide-Targeted Mesoporous Silica Nanoparticle-Supported Lipid Bilayers. *ACS Nano* **2012**, *6*, 2174−2188.

(7) Argyo, C.; Cauda, V.; Engelke, H.; Radler, J.; Bein, G.; Bein, T. Heparin-Coated Colloidal Mesoporous Silica Nanoparticles Efficiently Bind to Antithrombin as an Anticoagulant Drug-Delivery System. *Chem.—Eur. J.* **2012**, *18*, 428−432.

(8) Idris, N. M.; Gnanasammandhan, M. K.; Zhang, J.; Ho, P. C.; Mahendran, R.; Zhang, Y. In Vivo Photodynamic Therapy Using Upconversion Nanoparticles as Remote-Controlled Nanotransducers. *Nat. Med.* **2012**, *18*, 1580−1586.

(9) Li, X.; Chen, Y. J.; Wang, M. Q.; Ma, Y. J.; Xia, W. L.; Gu, H. C. A Mesoporous Silica Nanoparticle−PEI−Fusogenic Peptide System for siRNA Delivery in Cancer Therapy. *Biomaterials* **2013**, *34*, 1391−1401.

(10) Gu, J. L.; Liu, J. P.; Li, Y. S.; Zhao, W. R.; Shi, J. L. One-Pot Synthesis of Mesoporous Silica Nanocarriers with Tunable Particle Sizes and Pendent Carboxylic Groups for Cisplatin Delivery. *Langmuir* **2013**, *29*, 403−410.

(11) Knezevic, N. Z.; Trewyn, B. G.; Lin, V. S. Y. Light- and pH-Responsive Release of Doxorubicin from a Mesoporous Silica-Based Nanocarrier. *Chem.—Eur. J.* **2011**, *17*, 3338−3342.

(12) Li, Z. Y.; Liu, Y.; Wang, X. Q.; Liu, L. H.; Hu, J. J.; Luo, G. F.; Chen, W. H.; Rong, L.; Zhang, X. Z. One-Pot Construction of Functional Mesoporous Silica Nanoparticles for the Tumor-Acidity-Activated Synergistic Chemotherapy of Glioblastoma. *ACS Appl. Mater. Interfaces* **2013**, *5*, 7995−8001.

(13) Wu, S. H.; Hung, Y.; Mou, C. Y. Mesoporous Silica Nanoparticles as Nanocarriers. *Chem. Commun.* **2011**, *47*, 9972−9985.

(14) Orr, G. A.; Chrisler, W. B.; Cassens, K. J.; Tan, R.; Tarasevich, B. J.; Markillie, L. M.; Zangar, R. C.; Thrall, B. D. Cellular Recognition and Trafficking of Amorphous Silica Nanoparticles by Macrophage Scavenger Receptor A. *Nanotoxicology* **2011**, *5*, 296−311.

(15) Gualtieri, M.; Skuland, T.; Iversen, T. G.; Lag, M.; Schwarze, P.; Bilanicova, D.; Pojana, G.; Refsnes, M. Importance of Agglomeration State and Exposure Conditions for Uptake and Pro-Inflammatory Responses to Amorphous Silica Nanoparticles in Bronchial Epithelial Cells. *Nanotoxicology* **2012**, *6*, 700−712.

(16) Lundqvist, M.; Stigler, J.; Elia, G.; Lynch, I.; Cedervall, T.; Dawson, K. A. Nanoparticle Size and Surface Properties Determine the Protein Corona with Possible Implications for Biological Impacts. *Proc. Natl. Acad. Sci. U.S.A.* **2008**, *105*, 14265−14270.

(17) Tenzer, S.; Docter, D.; Rosfa, S.; Wlodarski, A.; Kuharev, J.; Rekik, A.; Knauer, S. K.; Bantz, C.; Nawroth, T.; Bier, C.; Sirirattanapan, J.; Mann, W.; Treuel, L.; Zellner, R.; Maskos, M.; Schild, H.; Stauber, R. H. Nanoparticle Size Is a Critical Physicochemical Determinant of the Human Blood Plasma Corona: A Comprehensive Quantitative Proteomic Analysis. *ACS Nano* **2011**, *5*, 7155−7167.

(18) Monopoli, M. P.; Bombelli, F. B.; Dawson, K. A. Nanobiotechnology: Nanoparticle Coronas Take Shape. *Nat. Nanotechnol.* **2011**, *6*, 11−12.

(19) Monopoli, M. P.; Aberg, C.; Salvati, A.; Dawson, K. A. Biomolecular Coronas Provide the Biological Identity of Nanosized Materials. *Nat. Nanotechnol.* **2012**, *7*, 779−786.

(20) Hayashi, Y.; Miclaus, T.; Scavenius, C.; Kwiatkowska, K.; Sobota, A.; Engelmann, P.; Scott-Fordsmand, J. J.; Enghild, J. J.; Sutherland, D. S. Species Differences Take Shape at Nanoparticles: Protein Corona Made of the Native Repertoire Assists Cellular Interaction. *Environ. Sci. Technol.* **2013**, *47*, 14367−14375.

(21) Huhn, D.; Kantner, K.; Geidel, C.; Brandholt, S.; De Cock, I.; Soenen, S. J. H.; Gil, P. R.; Montenegro, J. M.; Braeckmans, K.; Mullen, K.; Nienhaus, G. U.; Klapper, M.; Parak, W. J. Polymer-Coated Nanoparticles Interacting with Proteins and Cells: Focusing on the Sign of the Net Charge. *ACS Nano* **2013**, *7*, 3253−3263.

(22) Tenzer, S.; Docter, D.; Kuharev, J.; Musyanovych, A.; Fetz, V.; Hecht, R.; Schlenk, F.; Fischer, D.; Kiouptsi, K.; Reinhardt, C.; Landfester, K.; Schild, H.; Maskos, M.; Knauer, S. K.; Stauber, R. H. Rapid Formation of Plasma Protein Corona Critically Affects Nanoparticle Pathophysiology. *Nat. Nanotechnol.* **2013**, *8*, 772−U1000.

(23) Lesniak, A.; Salvati, A.; Santos-Martinez, M. J.; Radomski, M. W.; Dawson, K. A.; Aberg, C. Nanoparticle Adhesion to the Cell Membrane and Its Effect on Nanoparticle Uptake Efficiency. *J. Am. Chem. Soc.* **2013**, *135*, 1438−1444.

(24) Yan, Y.; Gause, K. T.; Kamphuis, M. M. J.; Ang, C. S.; O'Brien-Simpson, N. M.; Lenzo, J. C.; Reynolds, E. C.; Nice, E. C.; Caruso, F. Differential Roles of the Protein Corona in the Cellular Uptake of

Nanoporous Polymer Particles by Monocyte and Macrophage Cell Lines. *ACS Nano* **2013**, *7*, 10960−10970.
(25) Milani, S.; Bombelli, F. B.; Pitek, A. S.; Dawson, K. A.; Radler, J. Reversible versus Irreversible Binding of Transferrin to Polystyrene Nanoparticles: Soft and Hard Corona. *ACS Nano* **2012**, *6*, 2532−2541.
(26) Caracciolo, G.; Cardarelli, F.; Pozzi, D.; Salomone, F.; Maccari, G.; Bardi, G.; Capriotti, A. L.; Cavaliere, C.; Papi, M.; Lagana, A. Selective Targeting Capability Acquired with a Protein Corona Adsorbed on the Surface of 1,2-Dioleoyl-3-trimethylammonium Propane/DNA Nanoparticles. *ACS Appl. Mater. Interfaces* **2013**, *5*, 13171−13179.
(27) Lesniak, A.; Campbell, A.; Monopoli, M. P.; Lynch, I.; Salvati, A.; Dawson, K. A. Serum Heat Inactivation Affects Protein Corona Composition and Nanoparticle Uptake. *Biomaterials* **2010**, *31*, 9511−9518.
(28) Deng, Z. J.; Mortimer, G.; Schiller, T.; Musumeci, A.; Martin, D.; Minchin, R. F. Differential Plasma Protein Binding to Metal Oxide Nanoparticles. *Nanotechnology* **2009**, *20*, 455101.
(29) Lynch, I.; Salvati, A.; Dawson, K. A. Protein-Nanoparticle Interactions: What Does the Cell See? *Nat. Nanotechnol.* **2009**, *4*, 546−547.
(30) Walczyk, D.; Bombelli, F. B.; Monopoli, M. P.; Lynch, I.; Dawson, K. A. What the Cell "Sees" in Bionanoscience. *J. Am. Chem. Soc.* **2010**, *132*, 5761−5768.
(31) Monopoli, M. P.; Walczyk, D.; Campbell, A.; Elia, G.; Lynch, I.; Bombelli, F. B.; Dawson, K. A. Physical-Chemical Aspects of Protein Corona: Relevance to in Vitro and in Vivo Biological Impacts of Nanoparticles. *J. Am. Chem. Soc.* **2011**, *133*, 2525−2534.
(32) Mahmoudi, M.; Lynch, I.; Ejtehadi, M. R.; Monopoli, M. P.; Bombelli, F. B.; Laurent, S. Protein-Nanoparticle Interactions: Opportunities and Challenges. *Chem. Rev.* **2011**, *111*, 5610−5637.
(33) Jedlovszky-Hajdu, A.; Bombelli, F. B.; Monopoli, M. P.; Tombacz, E.; Dawson, K. A. Surface Coatings Shape the Protein Corona of SPIONs with Relevance to Their Application in Vivo. *Langmuir* **2012**, *28*, 14983−14991.
(34) Meerasa, A.; Huang, J. G.; Gu, F. X. Human Serum Lipoproteins Influence Protein Deposition Patterns on Nanoparticle Surfaces. *ACS Appl. Mater. Interfaces* **2013**, *5*, 489−493.
(35) Nel, A. E.; Madler, L.; Velegol, D.; Xia, T.; Hoek, E. M. V.; Somasundaran, P.; Klaessig, F.; Castranova, V.; Thompson, M. Understanding Biophysicochemical Interactions at the Nano-Bio Interface. *Nat. Mater.* **2009**, *8*, 543−557.
(36) Vertegel, A. A.; Siegel, R. W.; Dordick, J. S. Silica Nanoparticle Size Influences the Structure and Enzymatic Activity of Adsorbed Lysozyme. *Langmuir* **2004**, *20*, 6800−6807.
(37) Roach, P.; Farrar, D.; Perry, C. C. Surface Tailoring for Controlled Protein Adsorption: Effect of Topography at the Nanometer Scale and Chemistry. *J. Am. Chem. Soc.* **2006**, *128*, 3939−3945.
(38) Kecht, J.; Schlossbauer, A.; Bein, T. Selective Functionalization of the Outer and Inner Surfaces in Mesoporous Silica Nanoparticles. *Chem. Mater.* **2008**, *20*, 7207−7214.
(39) Cauda, V.; Schlossbauer, A.; Kecht, J.; Zurner, A.; Bein, T. Multiple Core-Shell Functionalized Colloidal Mesoporous Silica Nanoparticles. *J. Am. Chem. Soc.* **2009**, *131*, 11361−11370.
(40) Paula, A. J.; Montoro, L. A.; Souza Filho, A. G.; Alves, O. L. Towards Long-Term Colloidal Stability of Silica-Based Nanocarriers for Hydrophobic Molecules: Beyond the Stober Method. *Chem. Commun.* **2012**, *48*, 591−593.
(41) Stober, W.; Fink, A.; Bohn, E. Controlled Growth of Monodisperse Silica Spheres in Micron Size Range. *J. Colloid Interface Sci.* **1968**, *26*, 62−69.
(42) Xu, Y. M.; Zhan, C. Y.; Fan, L. H.; Wang, L.; Zheng, H. Preparation of Dual Crosslinked Alginate-Chitosan Blend Gel Beads and In Vitro Controlled Release in Oral Site-Specific Drug Delivery System. *Int. J. Pharm.* **2007**, *336*, 329−337.
(43) Brewer, S. H.; Glomm, W. R.; Johnson, M. C.; Knag, M. K.; Franzen, S. Probing BSA Binding to Citrate-Coated Gold Nanoparticles and Surfaces. *Langmuir* **2005**, *21*, 9303−9307.
(44) Zhang, X.; Servos, M. R.; Liu, J. W. Ultrahigh Nanoparticle Stability against Salt, pH, and Solvent with Retained Surface Accessibility via Depletion Stabilization. *J. Am. Chem. Soc.* **2012**, *134*, 9910−9913.
(45) Treuel, L.; Malissek, M.; Gebauer, J. S.; Zellner, R. The Influence of Surface Composition of Nanoparticles on their Interactions with Serum Albumin. *ChemPhysChem* **2010**, *11*, 3093−3099.
(46) Tian, M. H.; Lee, W. K.; Bothwell, M. K.; McGuire, J. Structural Stability Effects on Adsorption of Bacteriophage T4 Lysozyme to Colloidal Silica. *J. Colloid Interface Sci.* **1998**, *200*, 146−154.
(47) Pan, H.; Qin, M.; Meng, W.; Cao, Y.; Wang, W. How Do Proteins Unfold upon Adsorption on Nanoparticle Surfaces? *Langmuir* **2012**, *28*, 12779−12787.
(48) Lu, Z. X.; Cui, T.; Shi, Q. L. *Application of Circular Dichroism and Optical Rotatory Dispersion in Molecular Biology*; Science Press: Beijing, 1987.
(49) Roach, P.; Farrar, D.; Perry, C. C. Interpretation of Protein Adsorption: Surface-Induced Conformational Changes. *J. Am. Chem. Soc.* **2005**, *127*, 8168−8173.
(50) Wang, J.; Jensen, U. B.; Jensen, G. V.; Shipovskov, S.; Balakrishnan, V. S.; Otzen, D.; Pedersen, J. S.; Besenbacher, F.; Sutherland, D. S. Soft Interactions at Nanoparticles Alter Protein Function and Conformation in a Size Dependent Manner. *Nano Lett.* **2011**, *11*, 4985−4991.
(51) Puddu, V.; Perry, C. C. Peptide Adsorption on Silica Nanoparticles: Evidence of Hydrophobic Interactions. *ACS Nano* **2012**, *6*, 6356−6363.
(52) Graf, C.; Gao, Q.; Schutz, I.; Noufele, C. N.; Ruan, W. T.; Posselt, U.; Korotianskiy, E.; Nordmeyer, D.; Rancan, F.; Hadam, S.; Vogt, A.; Lademann, J.; Haucke, V.; Ruhl, E. Surface Functionalization of Silica Nanoparticles Supports Colloidal Stability in Physiological Media and Facilitates Internalization in Cells. *Langmuir* **2012**, *28*, 7598−7613.
(53) Orts-Gil, G.; Natte, K.; Thiermann, R.; Girod, M.; Rades, S.; Kalbe, H.; Thunemann, A. F.; Maskos, M.; Osterle, W. On the Role of Surface Composition and Curvature on Biointerface Formation and Colloidal Stability of Nanoparticles in a Protein-Rich Model System. *Colloids Surf., B* **2013**, *108*, 110−119.
(54) Orts-Gil, G.; Natte, K.; Drescher, D.; Bresch, H.; Mantion, A.; Kneipp, J.; Osterle, W. Characterisation of Silica Nanoparticles Prior to In Vitro Studies: from Primary Particles to Agglomerates. *J. Nanopart. Res.* **2011**, *13*, 1593−1604.
(55) Hoek, E. M. V.; Agarwal, G. K. Extended DLVO Interactions Between Spherical Particles and Rough Surfaces. *J. Colloid Interface Sci.* **2006**, *298*, 50−58.
(56) Patwardhan, S. V.; Emami, F. S.; Berry, R. J.; Jones, S. E.; Naik, R. R.; Deschaume, O.; Heinz, H.; Perry, C. C. Chemistry of Aqueous Silica Nanoparticle Surfaces and the Mechanism of Selective Peptide Adsorption. *J. Am. Chem. Soc.* **2012**, *134*, 6244−6256.
(57) Paula, A. J.; Martinez, D. S. T.; Araujo, R. T.; Souza, A. G.; Alves, O. L. Suppression of the Hemolytic Effect of Mesoporous Silica Nanoparticles after Protein Corona Interaction: Independence of the Surface Microchemical Environment. *J. Brazil. Chem. Soc.* **2012**, *23*, 1807−1814.
(58) Paula, A. J.; Araujo Junior, R. T.; Martinez, D. S. T.; Paredes Gamero, E. J.; Nader, H. B.; Duran, N.; Justo, G. Z.; Alves, O. L. Influence of Protein Corona on the Transport of Molecules into Cells by Mesoporous Silica Nanoparticles. *ACS Appl. Mater. Interfaces* **2013**, *5*, 8387−8393.
(59) Salvati, A.; Pitek, A. S.; Monopoli, M. P.; Prapainop, K.; Bombelli, F. B.; Hristov, D. R.; Kelly, P. M.; Aberg, C.; Mahon, E.; Dawson, K. A. Transferrin-Functionalized Nanoparticles Lose Their Targeting Capabilities when a Biomolecule Corona Adsorbs on the Surface. *Nat. Nanotechnol.* **2013**, *8*, 137−143.